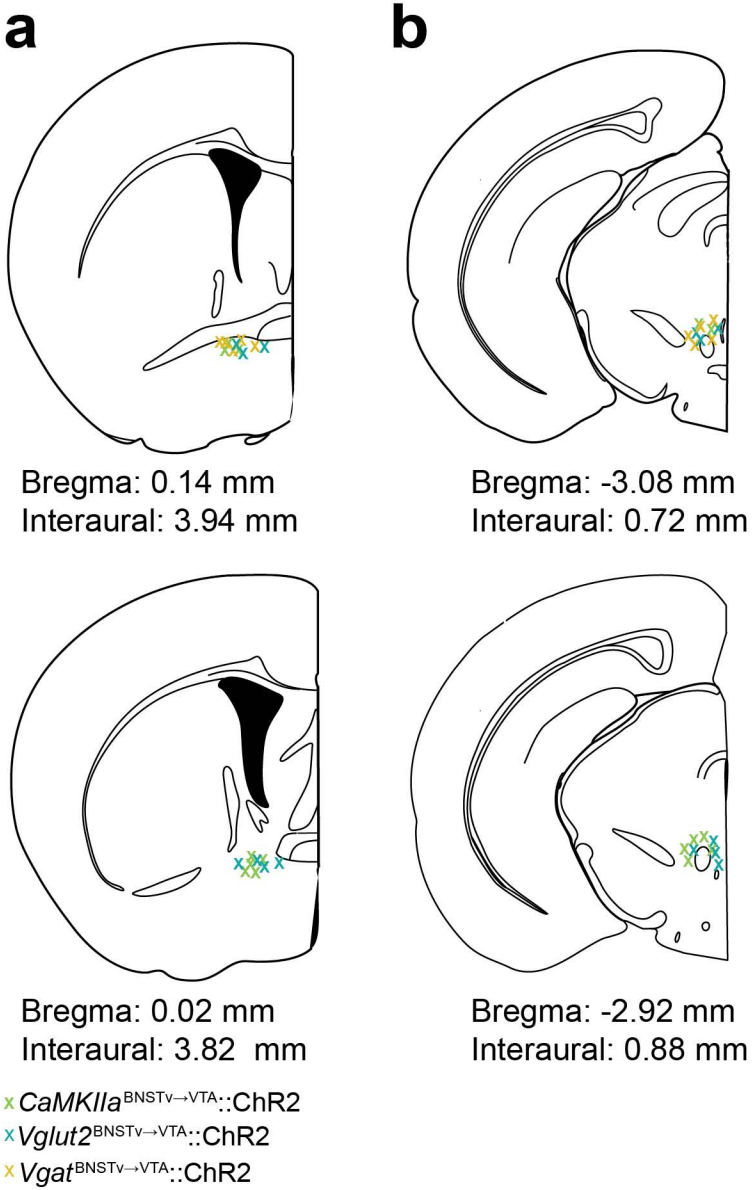

Supplementary Figure 1. Recording sites and optical fiber placements for optogenetic identification of BNSTv→VTA projection neurons. a - b. Location of multielectrode arrays within the BNSTv (**a**) and optical fibers within the VTA (**b**) based on histological examination of brain tissue following the experiments.

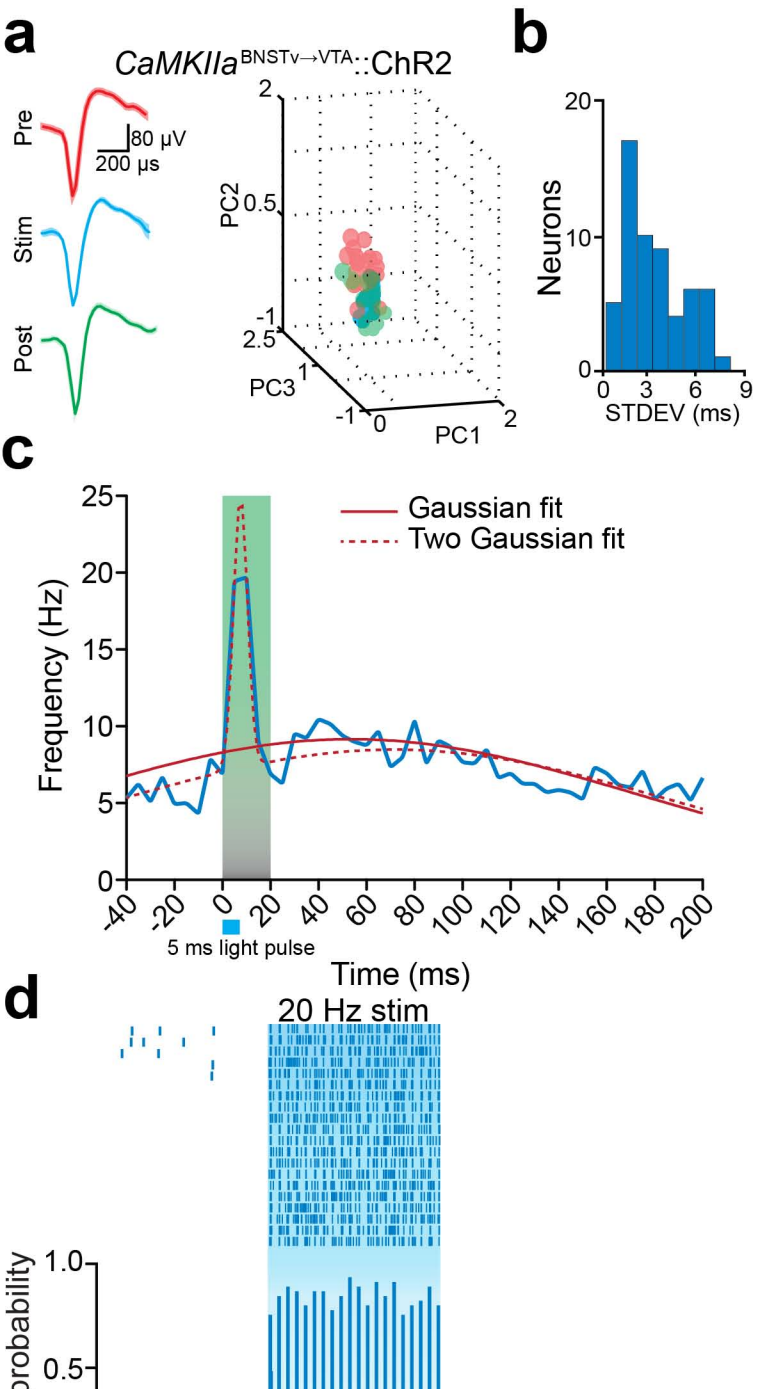

Supplementary Figure 2. Optogenetic identification of *CaMKIIa* $^{BNSTv→VTA}$ projection neurons in freely moving mice. **a.** Photostimulation does not alter recorded waveform shape during freely moving recordings (n = 53 units, n = 7 mice; PC: principle components, colored circles indicate waveform recorded during pre, during, or post stimulation epochs). **b.** Standard deviation (STDEV) spike latency after photostimulation for all identified projection neurons shown in Fig. 1j. **c.** Kolmogorov-Smirnov test for goodness of fit revealed the spike rate following antidromic photostimulation was not normally distributed ($P < 0.0001$; n = 53 units). Consistent with this, the data did not reliably fit a Gaussian distribution (R^2 = 0.2025), but was better encapsulated by a bimodal distribution using a sum of two Gaussian fit (R^2 = 0.8510). The two Gaussian model revealed distinct peaks in the fitted data occuring at t = 7.54 ms and t = 70.55 ms after the photostimulation onset. The peak occuring at 7.54 ms is indicitive of antidromic photostimulation, while the latter peak could represent transynaptic activity. **d.** Representative peri-event histogram and raster of a single unit responding reliably to high frequency antidromic photostimulation (5 ms pulse duration, 20 Hz, 1 s trial duration).

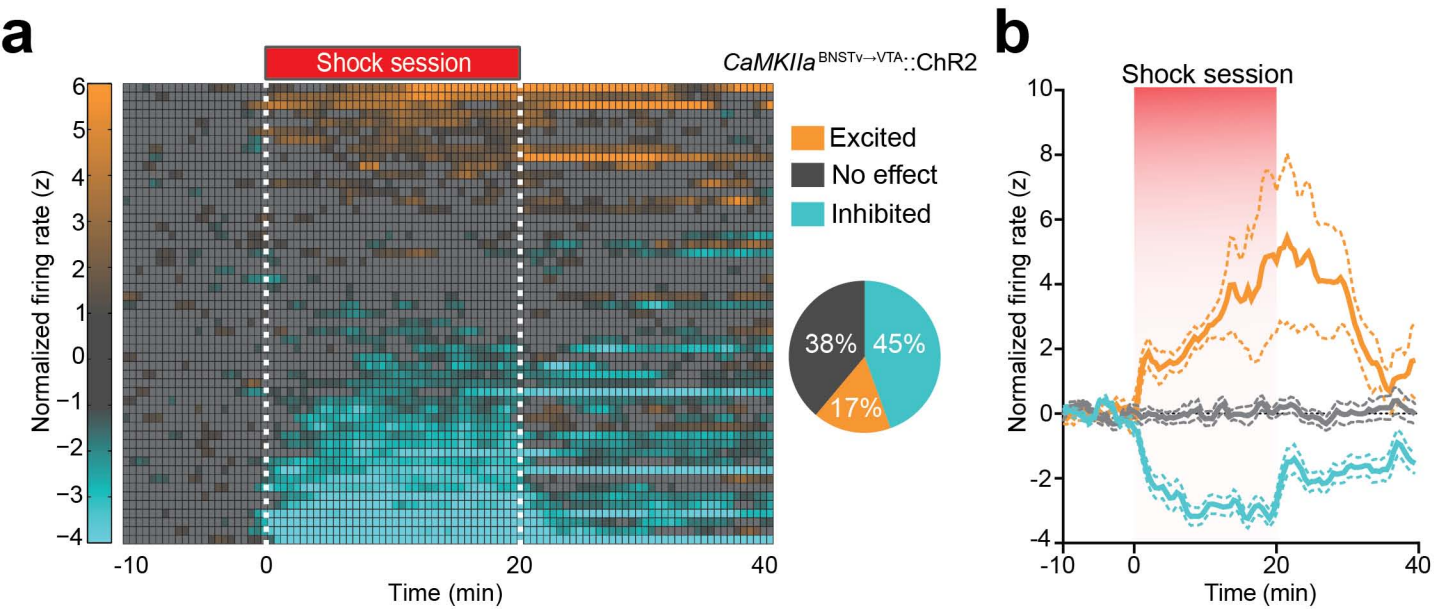

Supplementary Figure 3. BNSTv→VTA projection neurons differentially respond to aversive stimuli. a. Color plot and pie chart showing the normalized firing rates and classifications of all light responsive *CaMKIIa*$^{BNSTv→VTA}$ projection neurons (n = 53) during the foot-shock session. **b.** Average normalized firing rate of all classfied *CaMKIIa*$^{BNSTv→VTA}$ projection neurons are significantly altered during and following the foot-shock session ($F_{200, 5052}$ = 7.21, P < 0.0001). All values are ± s.e.m.

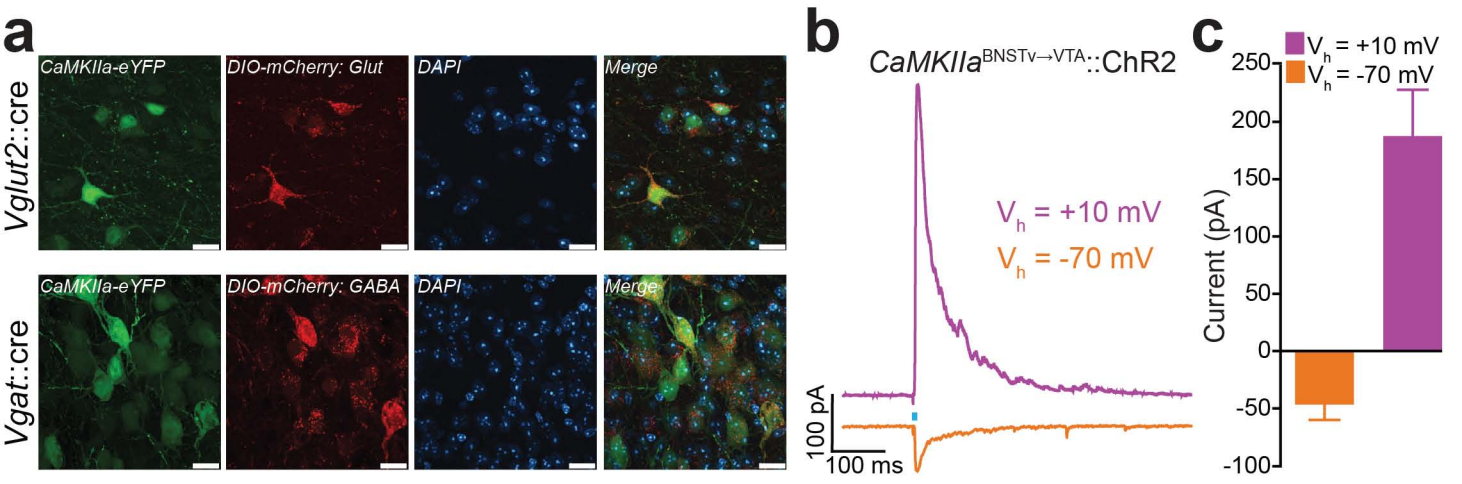

Supplementary Figure 4. Neurochemically distinct BNSTv cell types contain CaMKIIa and form functional excitatory and inhibitory synapses onto VTA neurons. a. AAV5-CaMKIIa-eYFP expression in both BNSTv-glutamatergic (top) and -GABAergic (bottom) neurons (scale bars = 20 µm). **b - c.** *CaMKIIa*$^{BNSTv \rightarrow VTA}$::ChR2 photostimulation resulted in inward currents at V_h = -70 mV and outward currents at V_h = +10 mV in VTA neurons (*n* = 11).

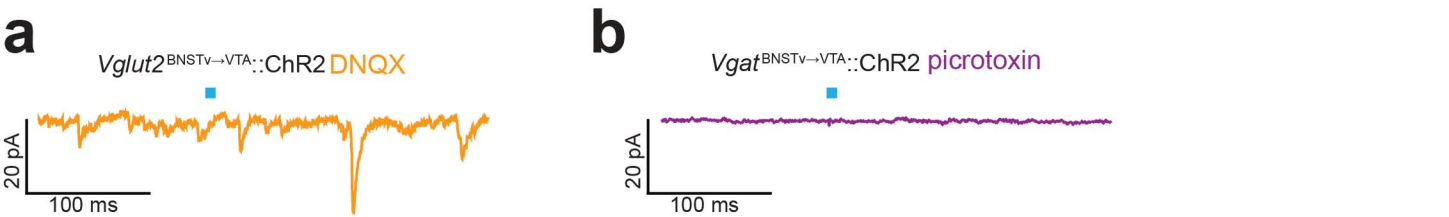

Supplementary Figure 5. Photostimulation of *Vglut2*$^{BNSTv→VTA}$::ChR2 and *Vgat*$^{BNSTv→VTA}$::ChR2 pathways produces excitatory and inhibitory currents respectively in VTA neurons. a. Current recorded from VTA neurons after photostimulation of *Vglut2*$^{BNSTv→VTA}$::ChR2 terminals after bath application of 10 μm DNQX with a cesium chloride internal solution, optimized to detect GABAergic mediated currents. 0/20 neurons exhibited timelocked responses to LED stimulation. However, spontaneous IPSCs are still detectable. **b.** Current recorded from VTA neurons after photostimulation of *Vgat*$^{BNSTv→VTA}$::ChR2 terminals after bath application of 10 μm picrotoxin with a cesium methanesulfonate internal solution, optimized to detect glutamatergic mediated currents. 0/20 neurons exhibited timelocked reponses to LED stimulation. All neurons were held at -70 mV.

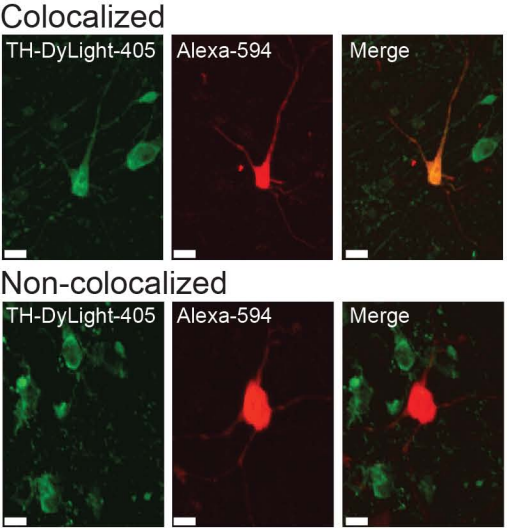

Supplementary Figure 6. Postsynaptic labeling of VTA neurons. Example confocal images of a non light-responsive TH+, VTA dopaminergic neuron (top) and a light-responsive nondopaminergic neuron (bottom) (scale bars = 20 μm).

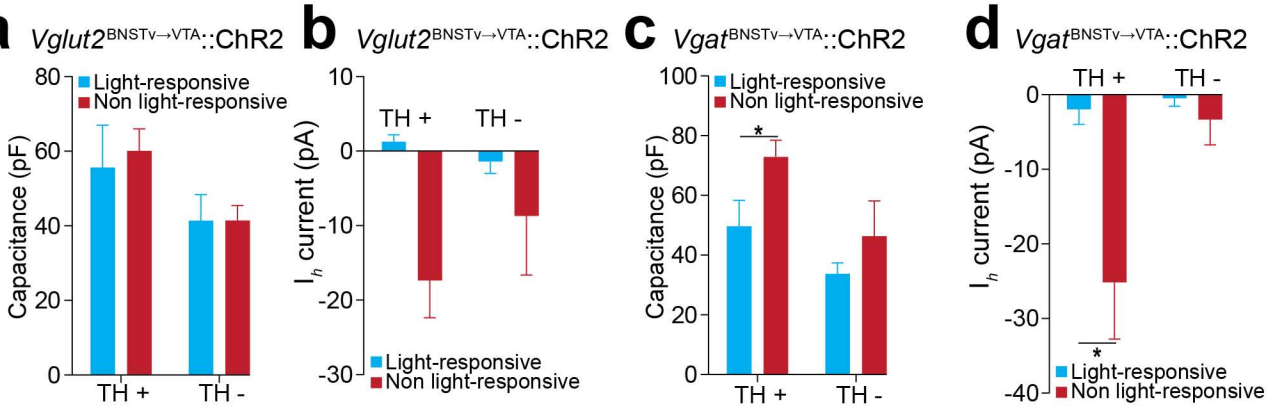

Supplementary Figure 7. *Vglut2*$^{BNSTv→VTA}$ and *Vgat*$^{BNSTv→VTA}$ terminals synapse onto non-dopaminergic and I_h negative dopaminergic neurons in the VTA. a - d. Membrane capacitance (pF) and I_h currents (pA) recorded from light-responsive (n = 3 - 9 cells per group) and non light-responsive (n = 16 - 26 cells per group) VTA dopaminergic neurons and light-responsive (n = 7 - 14 cells per group) and non light-responsive (n = 6 - 8 cells per group) non-dopaminergic neurons in *Vglut2*$^{BNSTv→VTA}$::ChR2 and *Vgat*$^{BNSTv→VTA}$::ChR2 mice. Whole-cell voltage-clamp recordings from VTA dopaminergic neurons in *Vgat*$^{BNSTv→VTA}$::ChR2 mice show that light-responsive neurons have significantly lower membrane capacitance (**c**; P = 0.027) as well as significantly lower I_h currents (**d**; P = 0.034) compared to non light-responsive neurons. All values are ± s.e.m. * $P < 0.05$, ** $P < 0.01$.

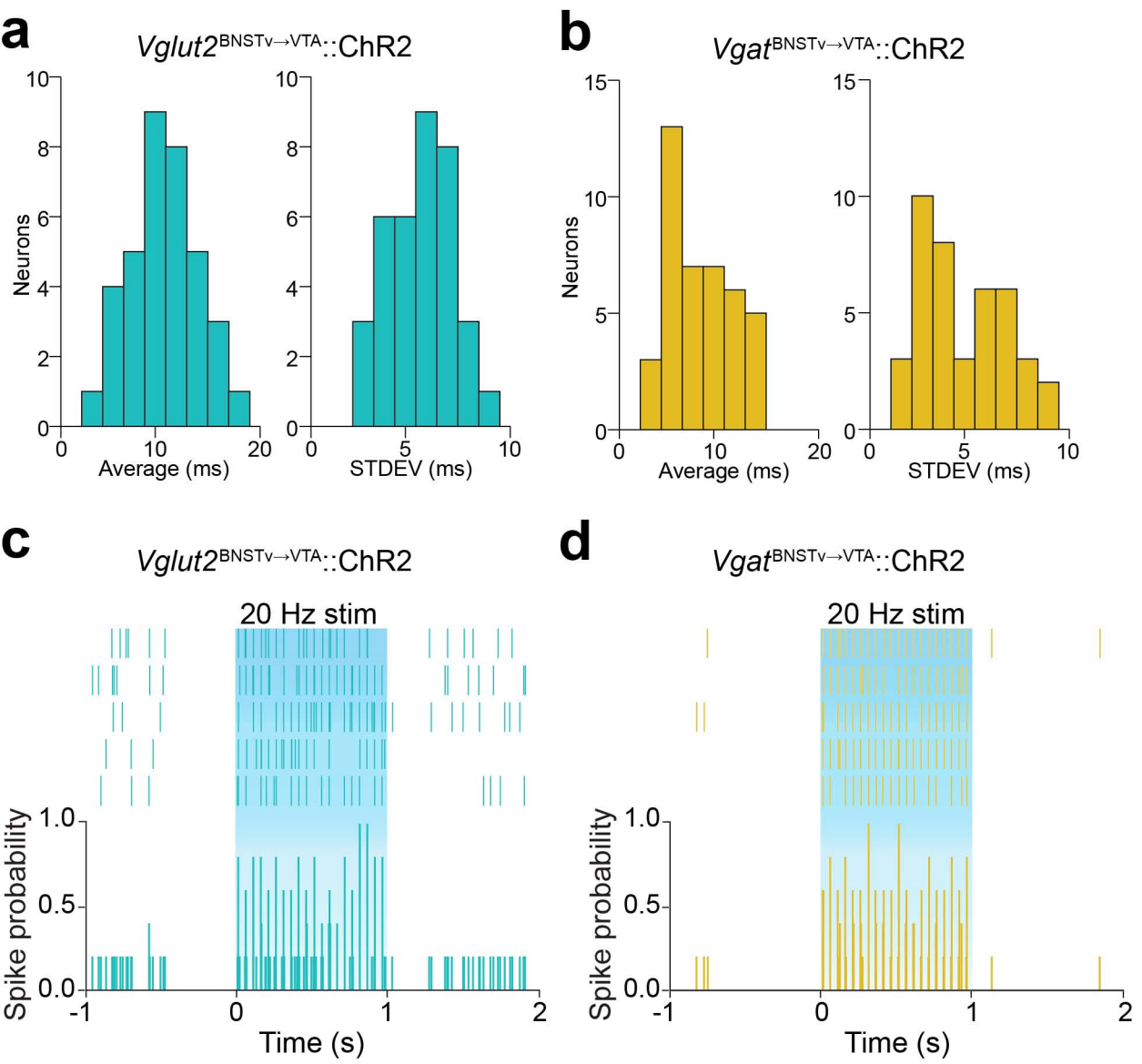

Supplementary Figure 8. Optogenetic identification of *Vglut2*$^{BNSTv→VTA}$ and *Vgat*$^{BNSTv→VTA}$ projection neurons. a - b. Mean spike latency (left) and standard deviation (STDEV; right) after 5 ms light-pulse delivery for all identified *Vglut2*$^{BNSTv→VTA}$ (*n* = 34) and *Vgat*$^{BNSTv→VTA}$ (*n* = 33) neurons in *Vglut2*$^{BNSTv→VTA}$::ChR2 (**a**) and *Vgat*$^{BNSTv→VTA}$::ChR2 (**b**) mice. **c - d.** Representative peri-event histogram and raster of a single unit from a *Vglut2*$^{BNSTv→VTA}$::ChR2 (**c**) and *Vgat*$^{BNSTv→VTA}$::ChR2 (**d**) mouse responding reliably to high frequency antidromic photostimulation (5 ms pulse duration, 20 Hz, 1 s trial duration).

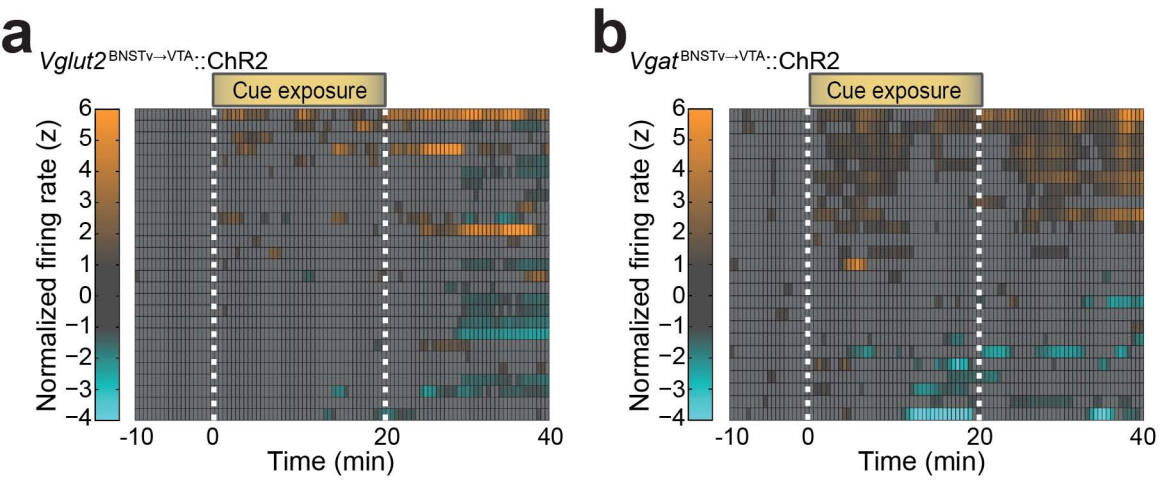

Supplementary Figure 9. Auditory and visual contextual cue presentations prior to the first foot-shock session do not drastically alter firing patterns of identified *Vglut2*$^{BNSTv→VTA}$ and *Vgat*$^{BNSTv→VTA}$ neurons. a - b. Color plots showing the normalized firing rate of $n = 27$ *Vglut2*$^{BNSTv→VTA}$ (**a**) and $n = 26$ *Vgat*$^{BNSTv→VTA}$ (**b**) neurons in response to unpaired auditory and visual contextual cue presentation ($n = 4$ mice per group).

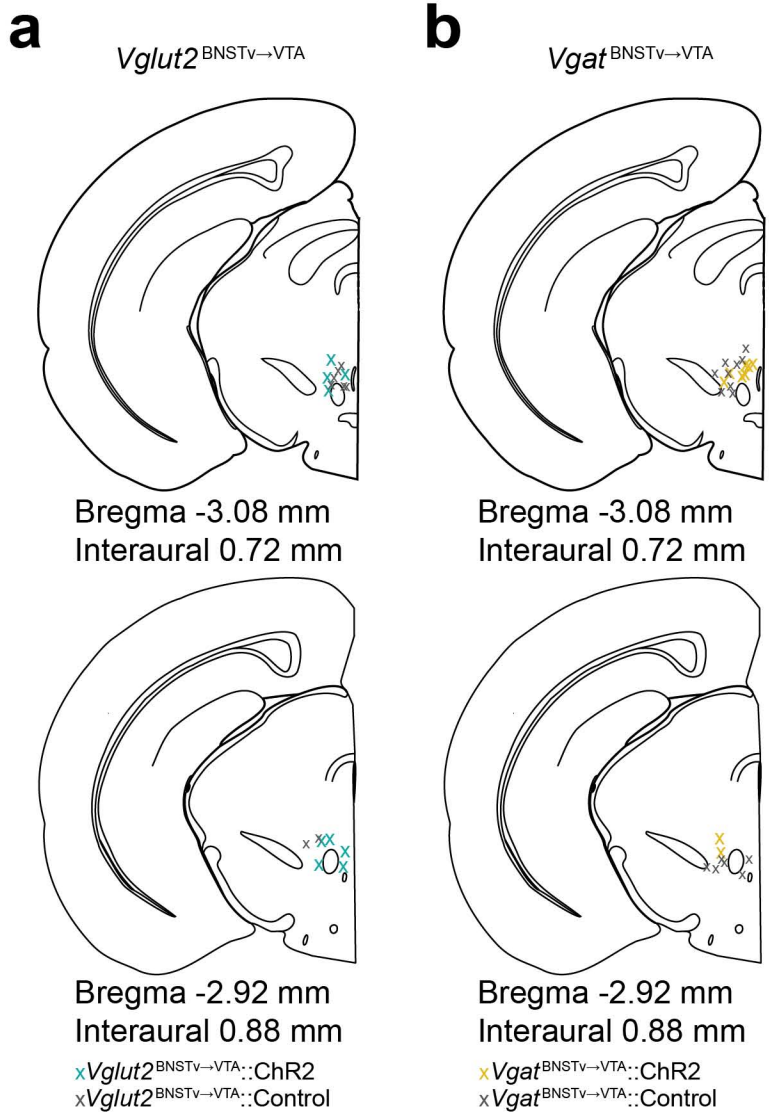

Supplementary Figure 10. Optical fiber stimulation sites within the VTA. a - b. Location of optical fibers within the VTA in the *Vglut2-ires-cre* mice (**a**) and the *Vgat-ires-cre* mice (**b**) based on histological examination of brain tissue following all behavioral experiments.

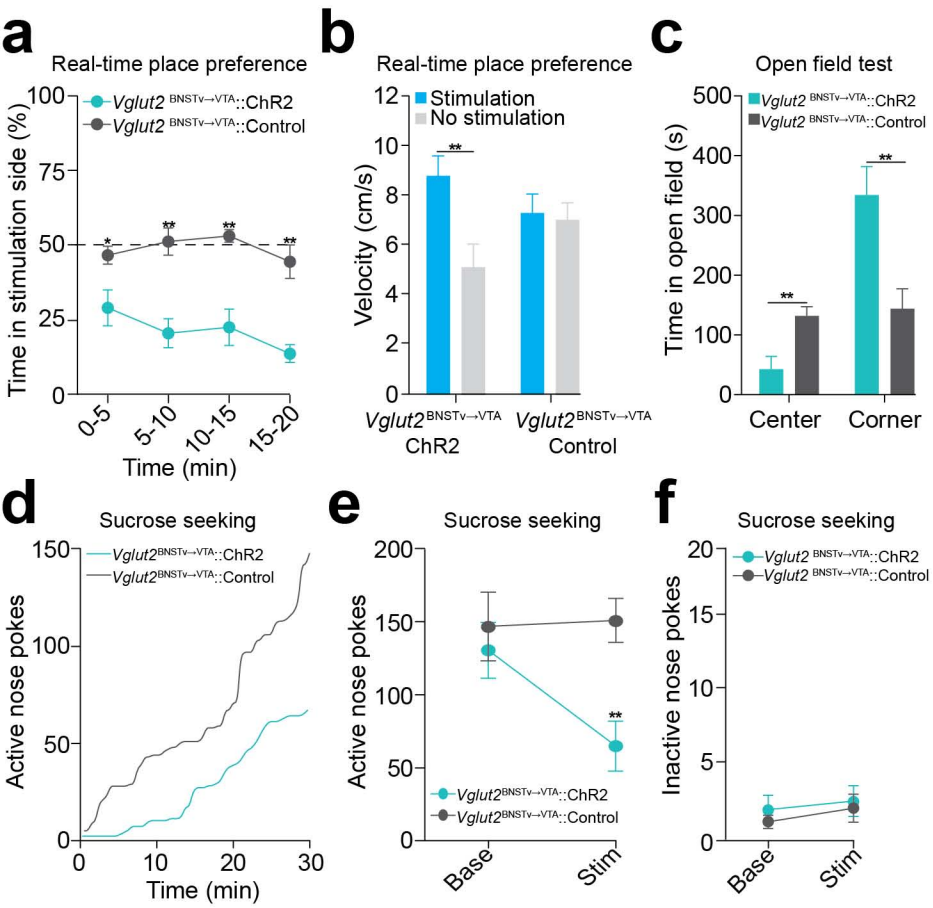

Supplementary Figure 11. Photostimulation of the *Vglut2*$^{BNSTv→VTA}$ pathway promotes aversion and anxiety-like behavior. **a.** *Vglut2*$^{BNSTv→VTA}$::ChR2 mice spent significantly less time in the stimulation side compared to *Vglut2*$^{BNSTv→VTA}$::Control mice ($F_{1,15}$ = 32.55, P < 0.001, n = 8 mice per group). **b.** *Vglut2*$^{BNSTv→VTA}$::ChR2 mice exhibited an increase in movement velocity (P = 0.005) in the stimulation side of a real-time place preference chamber. This effect was not observed in *Vglut2*$^{BNSTv→VTA}$::Control mice (n = 8 per group). **c.** Immediately following constant 20 Hz photostimulation of the *Vglut2*$^{BNSTv→VTA}$ pathway, *Vglut2*$^{BNSTv→VTA}$::ChR2 mice spent significantly less time in the center (P = 0.007) and significantly more time in the corners (P = 0.008) of an open-field chamber compared to *Vglut2*$^{BNSTv→VTA}$::Control mice, indicating increased anxiety-like behavior (n = 6 per group). **d.** Example cumulative records of active nose pokes made by representative *Vglut2*$^{BNSTv→VTA}$::ChR2 and *Vglut2*$^{BNSTv→VTA}$::Control mice to obtain a sucrose reward during constant 20 Hz photostimulation. **e.** *Vglut2*$^{BNSTv→VTA}$::ChR2 mice made significantly fewer nose pokes for a sucrose reward during constant 20 Hz photostimulation when compared to *Vglut2*$^{BNSTv→VTA}$::Control mice ($F_{1,12}$ = 13.09, P = 0.008; n = 7 mice per group). **f.** No significant differences were observed in inactive nose pokes between *Vglut2*$^{BNSTv→VTA}$::ChR2 and *Vglut2*$^{BNSTv→VTA}$::Control mice in a sucrose nose-poking task during constant 20 Hz photostimulation (n = 7 per group, P > 0.05). All values are ± s.e.m. * P < 0.05, ** P < 0.01.

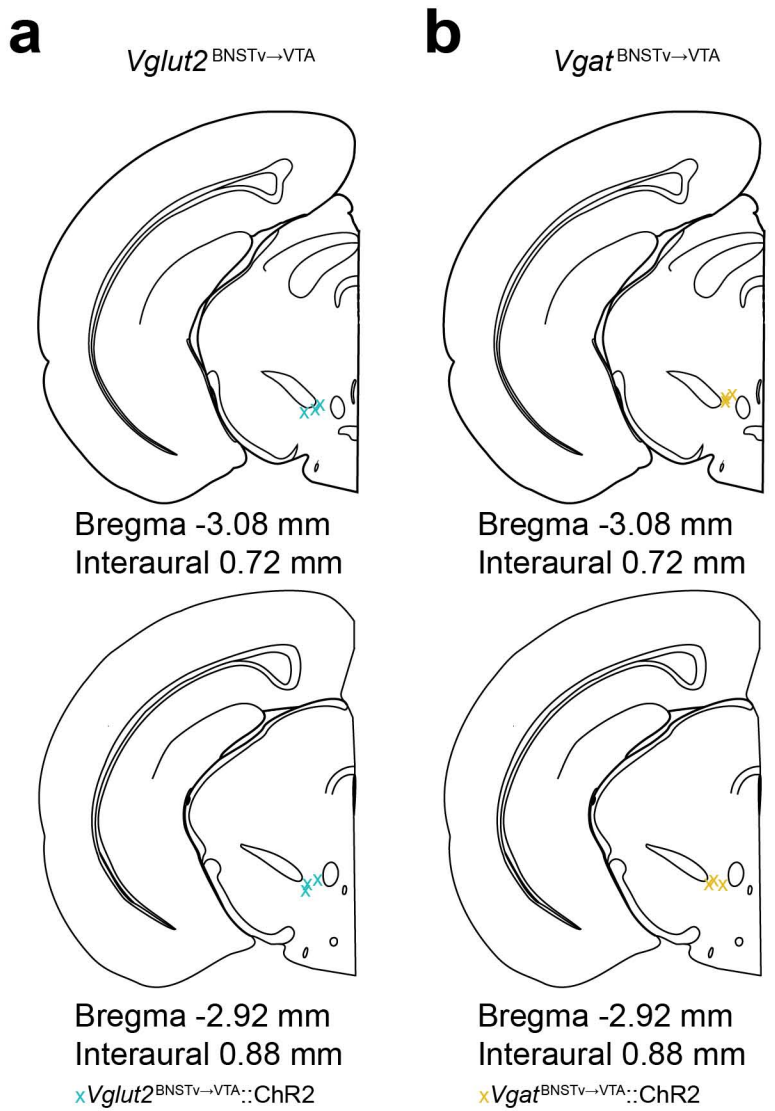

Supplementary Figure 12. Optical fiber stimulation and cannula microinjection sites within the VTA. a - b. Location of optical fibers and cannulae within the VTA in the *Vglut2* $^{BNSTv→VTA}$::ChR2 (**a**) and the *Vgat* $^{BNSTv→VTA}$::ChR2 (**b**) mice (*n* = 6 per group) based on histological examination of brain tissue following all behavioral experiments.

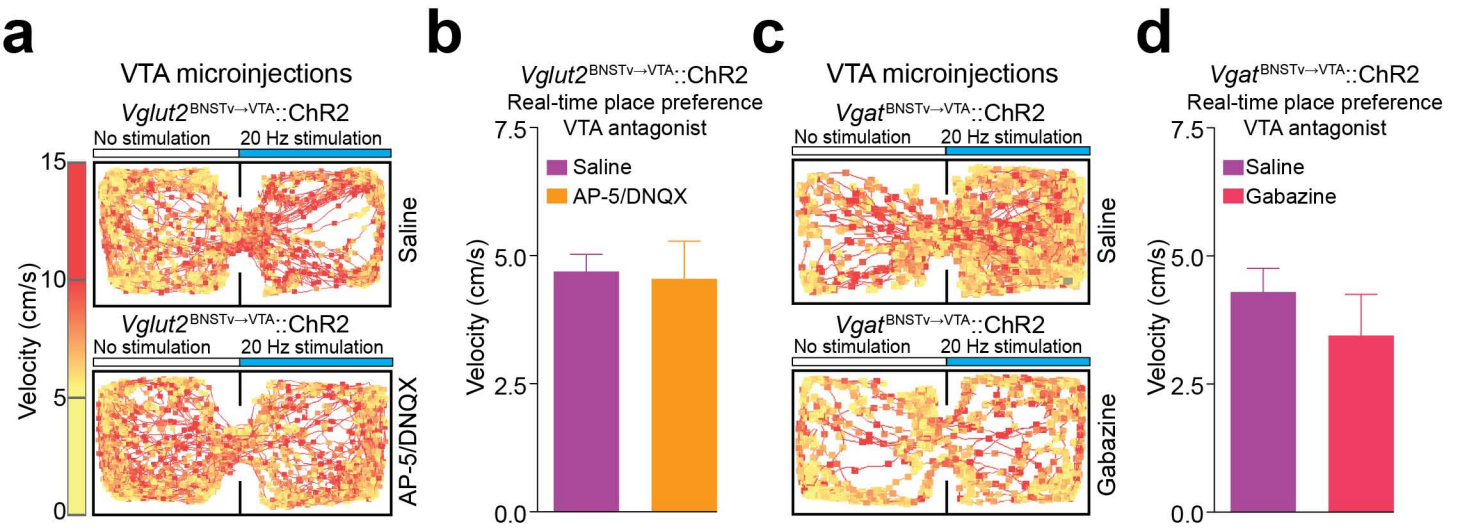

Supplementary Figure 13. Intra-VTA infusions of antagonists followed by *Vglut2*$^{BNSTv\rightarrow VTA}$::ChR2 pathway and *Vgat*$^{BNSTv\rightarrow VTA}$::ChR2 pathway photostimulation does not alter movement velocity. **a.** Real-time place preference representative tracks from a *Vglut2*$^{BNSTv\rightarrow VTA}$::ChR2 mouse after intra-VTA infusion of saline (top) and AP-5/DNQX (bottom). **b.** Intra-VTA infusions of AP-5/DNQX followed by *Vglut2*$^{BNSTv\rightarrow VTA}$::ChR2 pathway stimulation does not alter movement velocity in a real-time place preference paradigm compared to intra-VTA saline infusions (n = 6 mice). **c.** Real-time place preference representative tracks from a *Vgat*$^{BNSTv\rightarrow VTA}$::ChR2 mouse after intra-VTA infusion of saline (top) and Gabazine (bottom). **d.** Intra-VTA infusions of Gabazine followed by *Vgat*$^{BNSTv\rightarrow VTA}$::ChR2 pathway stimulation does not alter movement velocity in a real-time place preference paradigm compared to intra-VTA saline infusions (n = 6 mice). All values are ± s.e.m.

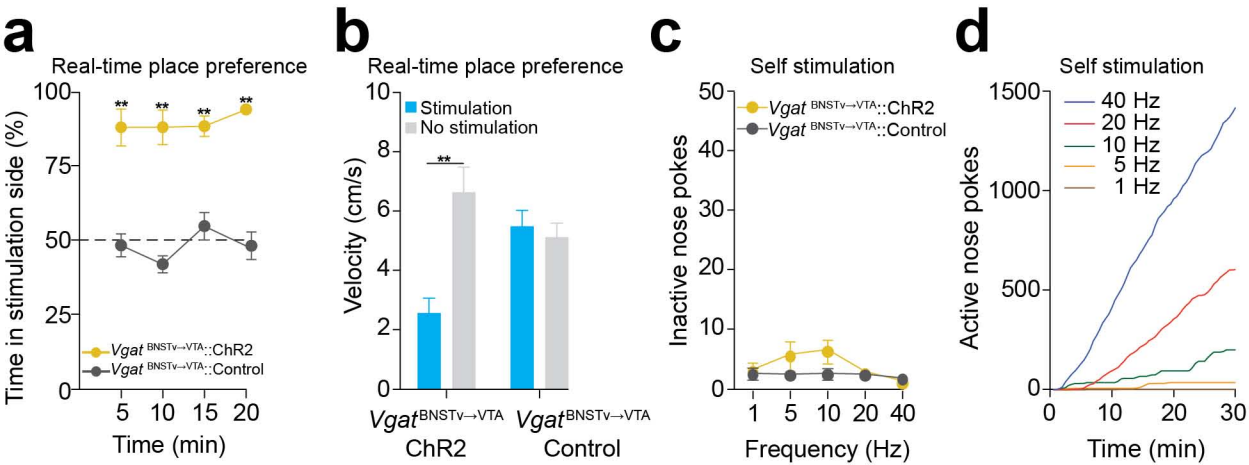

Supplementary Figure 14. Photostimulation of the *Vgat*$^{BNSTv→VTA}$ pathway promotes reward-related behaviors. a. *Vgat*$^{BNSTv→VTA}$::ChR2 mice spent significantly more time in the stimulation side when compared to *Vgat*$^{BNSTv→VTA}$::Control mice ($F_{1,13}$ = 89.56, P < 0.001; n = 7 - 8 mice per group). **b.** *Vgat*$^{BNSTv→VTA}$::ChR2 mice exhibited a decrease in movement velocity (P = 0.004) in the stimulation side of a real-time place preference chamber. This effect was not observed in *Vgat*$^{BNSTv→VTA}$::Control mice (n = 7 - 8 per group). **c.** No significant differences were observed for inactive nose pokes between *Vgat*$^{BNSTv→VTA}$::ChR2 and *Vgat*$^{BNSTv→VTA}$::Control mice at all frequencies tested (n = 5 - 7 per group, P > 0.05). **d.** Example cumulative records of active nose pokes performed by a *Vgat*$^{BNSTv→VTA}$::ChR2 mouse to obtain photostimulation over a range of frequencies. All values are ± s.e.m. ** P < 0.01.

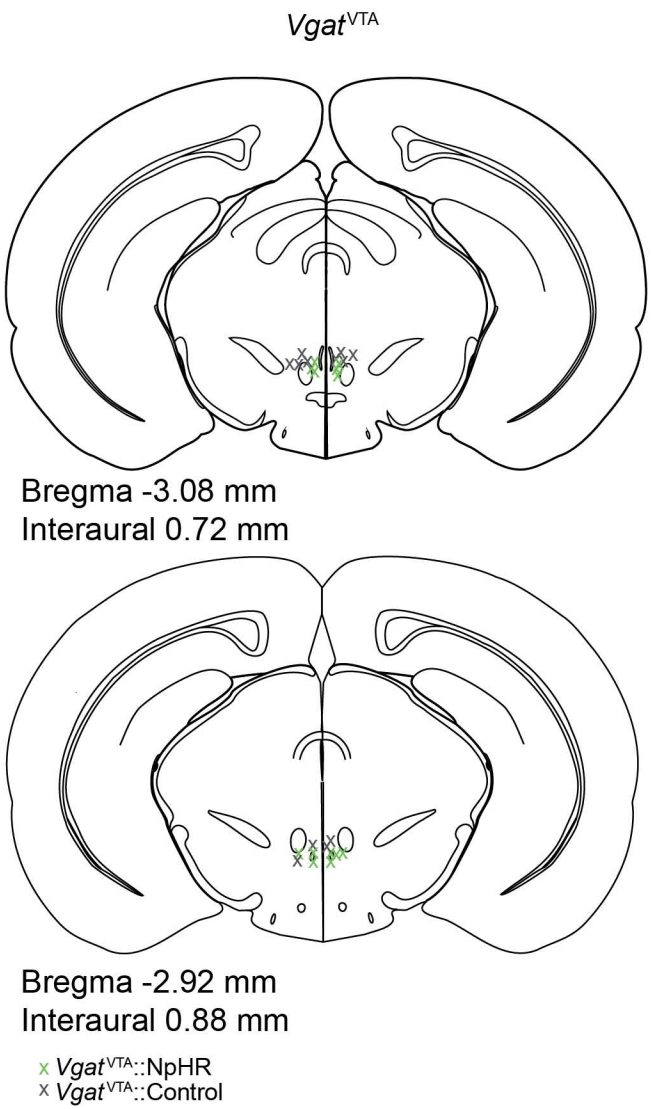

Supplementary Figure 15. Optical fiber inhibition sites within the VTA. Location of bilateral optical fibers within the VTA in *Vgat-ires-cre* mice (*n* = 6 mice per group) based on histological examination of brain tissue following all behavioral experiments.

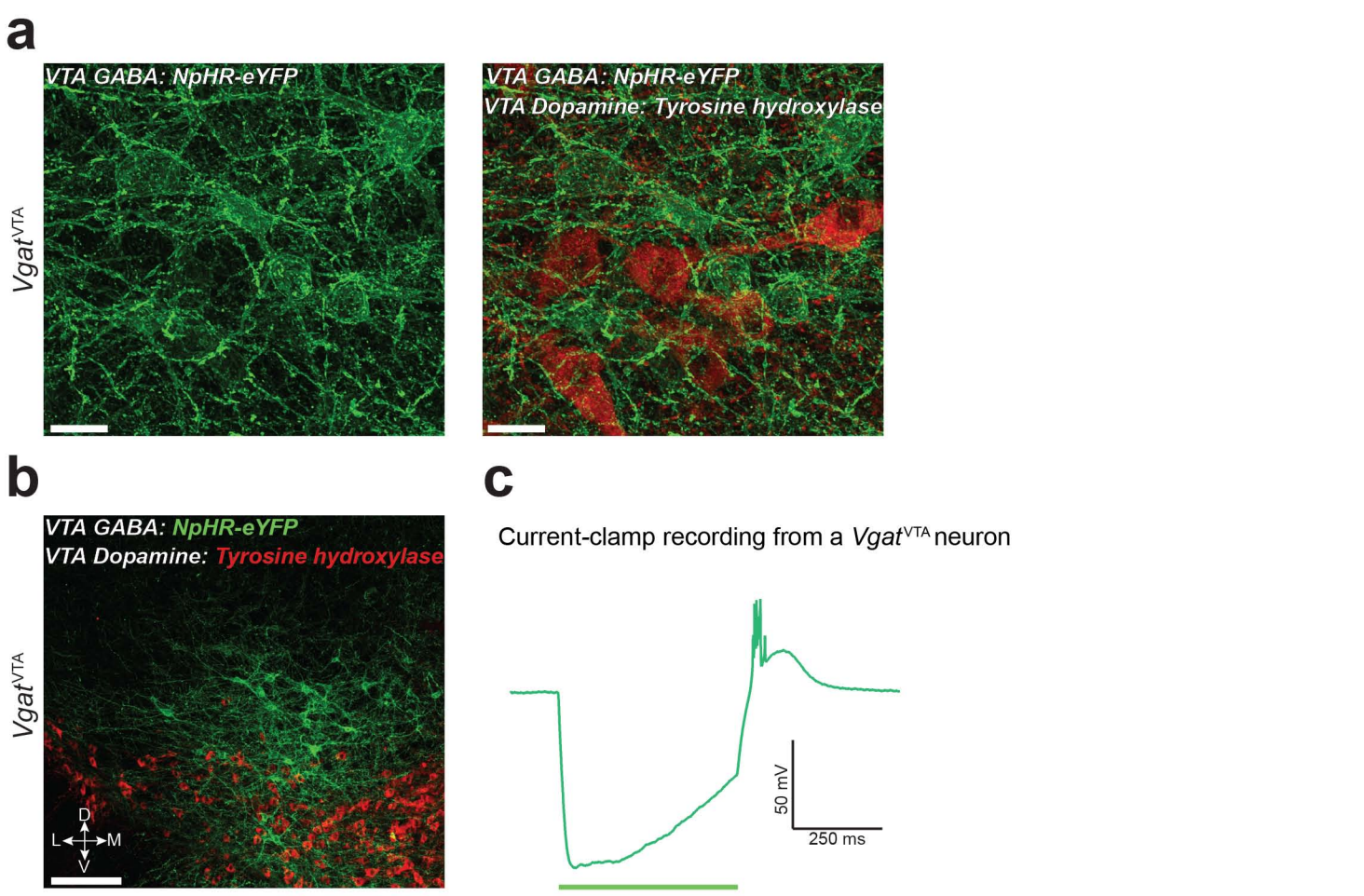

Supplementary Figure 16. Photoinhibition of *Vgat*^{VTA} neurons. **a.** 63x confocal image showing expression of NpHR-eYFP (green) in *Vgat*^{VTA} neurons (left) and tyrosine hydroxylase (TH) (right). (Scale = 20 µm). **b.** 20x confocal image showing expression of NpHR-eYFP in *Vgat*^{VTA} neurons following injection of the viral construct into the VTA, shown in green. VTA dopaminergic neurons, as indicated by TH immunoreactivity, are shown in red (D, dorsal; V, ventral; L, lateral; M, medial; Scale = 200 µm). **c.** Example whole-cell current clamp recording showing robust membrane hyperpolarization after a 500 ms light pulse (532 nm) in a VTA neuron expressing NpHR. Average hyperpolarization of membrane = -52.95 ± 11.95 mV in n = 4 neurons.

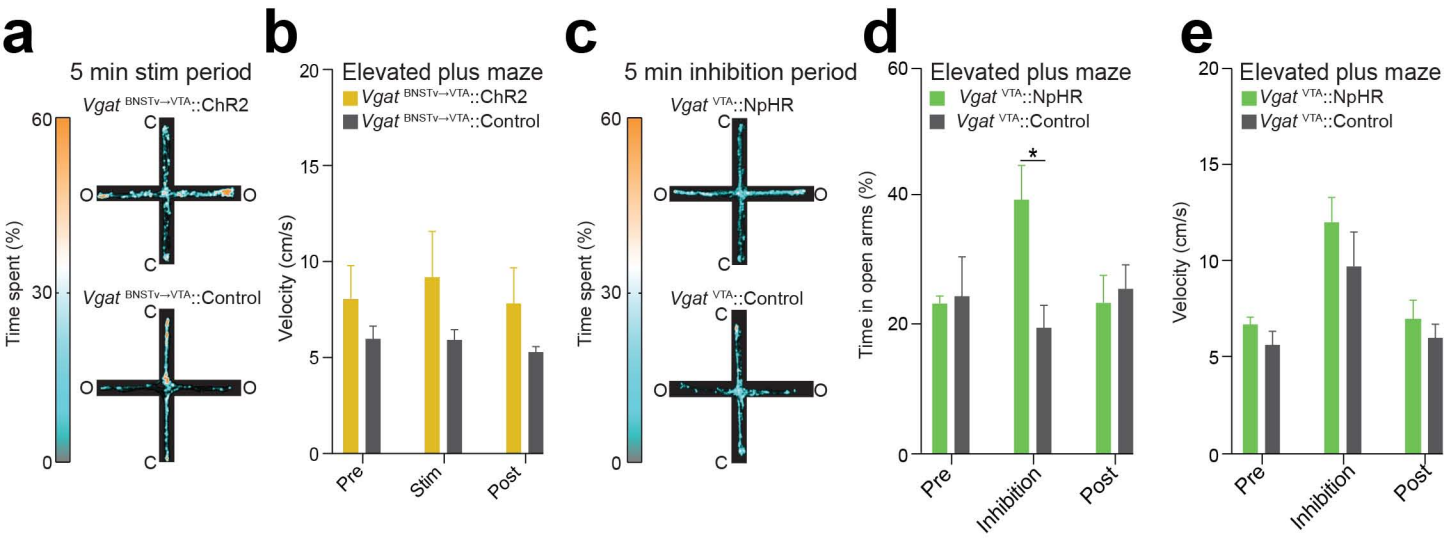

Supplementary Figure 17. Photostimulation of the *Vgat*$^{BNSTv→VTA}$ pathway and photoinhibition of *Vgat*^{VTA} neurons produces anxiolysis and does not alter movement velocity. **a.** Representative heat maps displaying average time spent in the elevated plus maze during the 5 min photostimulation epoch from *Vgat*$^{BNSTv→VTA}$::ChR2 (top) and *Vgat*$^{BNSTv→VTA}$::Control (bottom) mice (O, open arm; C, closed arm). **b.** No significant differences were observed in movement velocity between *Vgat*$^{BNSTv→VTA}$::ChR2 and *Vgat*$^{BNSTv→VTA}$::Control mice (n = 7 mice per group) during each time epoch on the elevated plus maze. **c.** Representative heat maps dispalying average time spent in the elevated plus maze during the 5 min photoinhibition epoch from *Vgat*^{VTA}::NpHR (top) and *Vgat*^{VTA}::Control (bottom) mice. **d.** *Vgat*^{VTA}::NpHR mice spent significantly more time in the open arms compared to *Vgat*^{VTA}::Control mice (n = 5 mice per group) during the 5 min photoinhibition epoch $F_{2,16}$ = 10.519, P < 0.01. **e.** No significant differences were observed in movement velocity between *Vgat*^{VTA}::NpHR and *Vgat*^{VTA}::Control mice (n = 5 mice per group) during each time epoch on the elevated plus maze. All values are ± s.e.m. * P < 0.05.

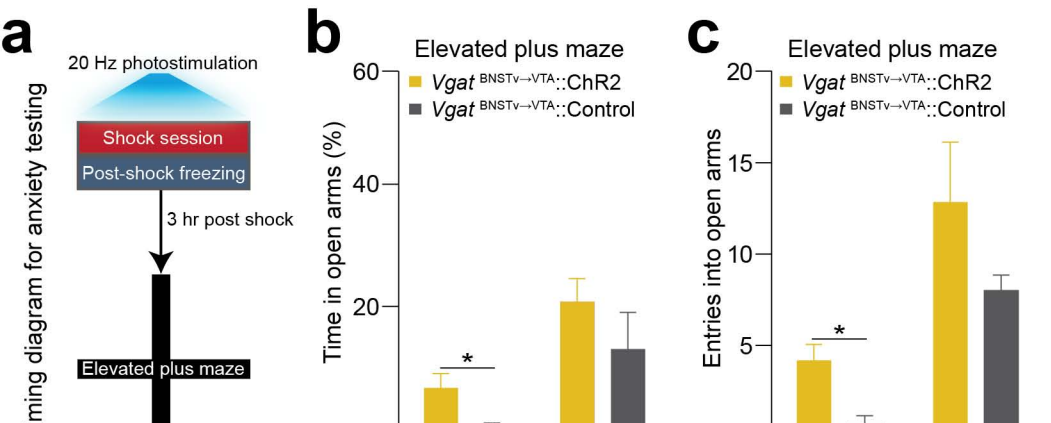

Supplementary Figure 18. Photostimulation of the *Vgat*$^{BNSTv→VTA}$ pathway buffers stress-induced anxiety. a. Schematic of shock-induced anxiety paradigm. **b - c.** 3 hr after shock exposure, *Vgat*$^{BNSTv→VTA}$::ChR2 mice spent significantly more time in the open arms ($F_{1,20}$ = 12.822, P = 0.002, P = 0.03) and made significantly more open-arm entries ($F_{1,20}$ = 20.3771, P < 0.001, P = 0.008) compared to *Vgat*$^{BNSTv→VTA}$::Control mice (n = 6 - 7 per group). Photostimulation in *Vgat*$^{BNSTv→VTA}$::ChR2 and *Vgat*$^{BNSTv→VTA}$::Control mice in the absence of foot shock resulted in no significant differences. All values are ± s.e.m. * P < 0.05.

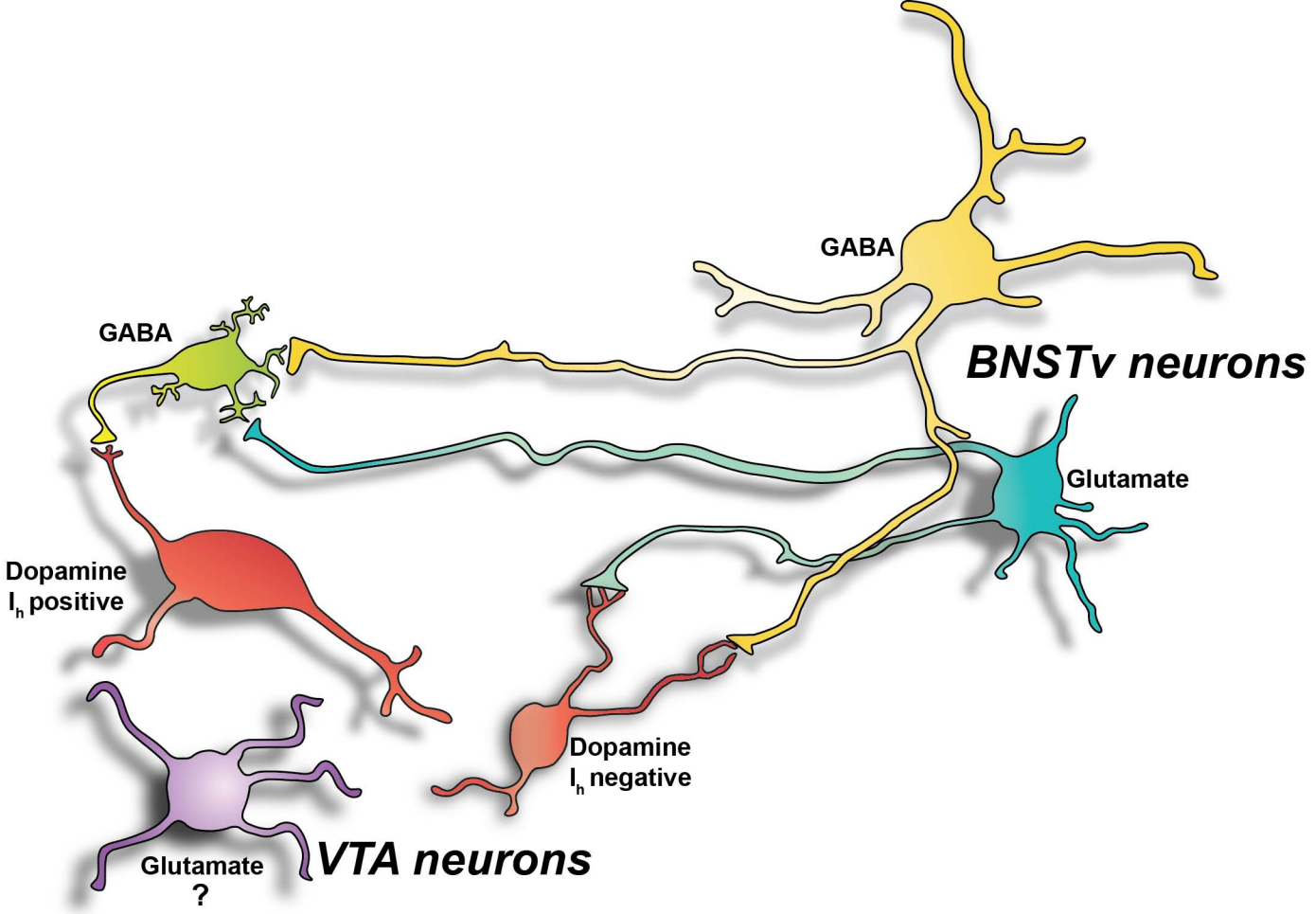

Supplementary Figure 19. **Genetically distinct BNSTv→VTA projections bidirectionally modulate discrete VTA neurons through indirect and direct mechanisms.** Summary schematic detailing how *Vgat*$^{BNSTv→VTA}$ and *Vglut2*$^{BNSTv→VTA}$ projection neurons regulate VTA circuit function through direct innervation as well as through indirect stimulation and inhibition of VTA dopaminergic neurons.

Table S1. Spontaneous waveform are highly correlated to light-evoked waveforms

CaMKIIa$^{BNSTv \rightarrow VTA}$ projection neurons

Analysis	Waveform shape			Prinicpal component analysis		
Comparison	Pre/Stim	Stim/Post	Pre/Post	Pre/Stim	Stim/Post	Pre/Post
r	0.95 ± 0.01	0.95 ± 0.01	0.95 ± 0.01	0.94 ± 0.02	0.91 ± 0.03	0.93 ± 0.04

n = 53

Vglut2$^{BNSTv \rightarrow VTA}$ projection neurons

Analysis	Waveform shape			Prinicpal component analysis		
Comparison	Pre/Stim	Stim/Post	Pre/Post	Pre/Stim	Stim/Post	Pre/Post
r	0.91 ± 0.01	0.90 ± 0.01	0.90 ± 0.01	0.92 ± 0.02	0.92 ± 0.02	0.95 ± 0.01

n = 34

Vgat$^{BNSTv \rightarrow VTA}$ projection neurons

Analysis	Waveform shape			Prinicpal component analysis		
Comparison	Pre/Stim	Stim/Post	Pre/Post	Pre/Stim	Stim/Post	Pre/Post
r	0.92 ± 0.01	0.92 ± 0.01	0.92 ± 0.01	0.94 ± 0.02	0.91 ± 0.03	0.97 ± 0.01

n = 33